한국지진공학회 논문집 20권 6호 (통권 제112호)
2016년 11월

ISSN 1226-525X / eISSN 2234-1099
EESK J Earthquake Eng Vol. 20 No. 6, 379-389
http://dx.doi.org/10.5000/EESK.2016.20.6.379

지반-구조물 상호작용이 면진 원전구조물의 지진응답에 미치는 영향 평가

Evaluation of the Soil-structure Interaction Effect on Seismically Isolated Nuclear Power Plant Structures

이은행[1)]* · 김재민[2)] · 주광호[3)] · 김현욱[4)]

Lee, Eun-haeng[1)]* · Kim, Jae-min[2)] · Joo, Kwang-ho[3)] · Kim, Hyun-uk[3)]

[1)]전남대학교 대학원 건설환경공학과, 박사과정, [2)]전남대학교 해양토목공학과, 교수, [3)]한국수력원자력 중앙연구원

[1)]Department of Civil and Environmental Engineering, Chonnam National University, [2)]Department of Marine and Civil Engineering, Chonnam National University, [3)]Central Research Institute of KHNP

/ ABSTRACT /

This study intends to evaluate the conservativeness of the fixed-base analysis as compared to the soil-structure interaction (SSI) analysis for the seismically isolated model of a nuclear power plant in Korea. To that goal, the boundary reaction method (BRM), combining frequency-domain and time-domain analyses in a twofold process, is adopted for the SSI analysis considering the nonlinearity of the seismic base isolation. The program KIESSI-3D is used for computing the reaction forces in the frequency domain and the program MIDAS/Civil is applied for the nonlinear time-domain analysis. The BRM numerical model is verified by comparing the results of the frequency-domain analysis and time-domain analysis for the soil-structure system with an equivalent linear base isolation model. Moreover, the displacement response of the base isolation and the horizontal response at the top of the structure obtained by the nonlinear SSI analysis using BRM are compared with those obtained by the fixed-base analysis. The comparison reveals that the fixed-base analysis provides conservative peak deformation for the base isolation but is not particularly conservative in term of the floor response spectrum of the superstructure.

Key words: Base-isolated NPP, Nonlinear SSI analysis, Fixed-base analysis, Seismic analysis

1. Introduction

The seismic isolation technology reached its maturity and started to be used extensively in structures like buildings and bridges after 1970s[1,2] and has recently been studied for application in special structures like nuclear power plant structures[3-6]. Seismic isolation has been already applied in nuclear facilities like the Cruas nuclear power plant in France and the Koeberg nuclear power station in South Africa. It is also under construction at the site of the Cadarache nuclear power plant in France[7]. The seismic design of seismically isolated nuclear facilities necessitates imperatively the consideration of not only the nonlinearity of the members like the seismic isolation but also of the soil-structure interaction (SSI)[8-10].

Besides, various studies compared the SSI effect and fixed-base analysis results of seismically isolated structures[11-17]. All these previous studies reported that the response of the superstructure computed by considering the SSI effect was larger than that obtained under fixed-base condition. On the other hand, for the computed displacement response of the nonlinear elements including the seismic isolation, several studies found out fixed-base response larger than the SSI response [13] while other studies concluded the contrary[14,17]. Accordingly, it is necessary to examine precisely the SSI effect on the nonlinear displacement response of the seismic isolation in large and complex seismically isolated structures like nuclear facilities.

The classical approach to solve a nonlinear SSI problem is the hybrid time-domain analysis combining the frequency-domain analysis

*Corresponding author: Kim, Jae-min
E-mail: jm4kim@jnu.ac.kr
(Received March 22, 2016; Revised May 12, 2016; Accepted July 6, 2016)

and the time-domain analysis[18-20]. Recently, a method using concurrently the DRM (Domain Reduction Method)[21] and the PML (Perfectly Matched Layer)[22] has been developed[23,24], and is supported as a function by the LS-DYNA program[25]. Though, it is still realistically difficult to achieve such SSI analysis by means of multi-purposed finite element analysis programs. In practice, the BRM (Boundary Reaction Method) was proposed as an analysis technique avoiding the need of an iterative process for the consideration of the nonlinear SSI effect[26-29]. This method can be exploited for the nonlinear SSI analysis of seismically isolated nuclear facilities by combining both linear SSI analysis in the frequency-domain and time-domain finite element analysis enabling to perform nonlinear analysis.

The level of the design seismic load for the current standard nuclear power plant of Korea corresponds to a peak ground acceleration (PGA) of 0.3g but should be augmented to 0.5g for zones with high seismic risks[30]. However, such increase of the PGA requires tremendous efforts and time since the seismic design of the Korean standard NPP model should be completely revised. Accordingly, research is also actively conducted in Korea on an alternative applying seismic isolation in the nuclear reactor so as to reduce the effective seismic load transmitted to the nuclear structures and to secure their seismic safety[31].

This study intends to evaluate the conservativeness of the fixed-base analysis as compared to the SSI analysis for the seismically isolated model of a nuclear power plant. For this purpose, the nonlinear seismic response of a seismically isolated NPP under fixed-base condition is compared to the one considering the SSI effect. BRM is applied for the SSI analysis considering the nonlinearity of the seismic isolation. Since the reliability of the linear analysis model should be secured in order to achieve exact nonlinear SSI analysis using BRM, the response obtained by BRM for a linear analysis problem assuming the seismic isolation as an equivalent linear model is verified through comparison with the response obtained by the common seismic analysis. After verification of the linear model, nonlinear SSI analysis using BRM is performed and the corresponding results are compared to those of the fixed-base analysis.

2. Analysis model

2.1 Numerical model of seismically isolated NPP structures

This study adopted a seismically isolated NPP model developed for research purpose by Kim and Lee [32] as shown in Fig. 1(b) which is a simplified model of Fig. 1(a) by Han et al.[30]. The properties of the NPP model are given in Table 1. The bottom of a basemat is fixed and the results of the eigenvalue analysis are summarized in Table 2. The

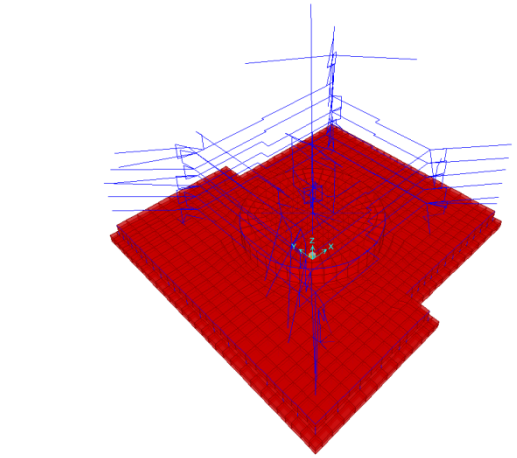

(a) Original NPP model (Han et al., 2015)

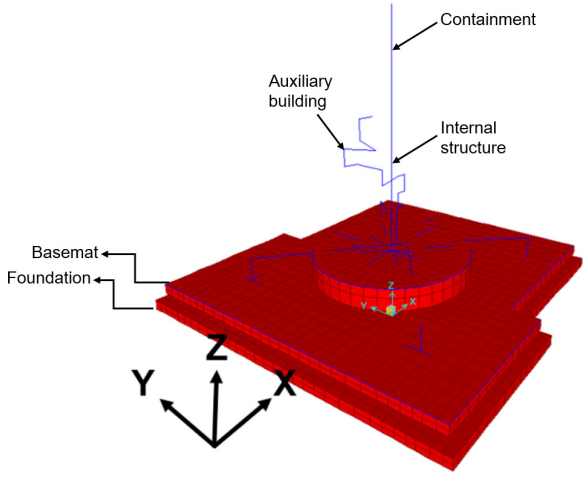

(b) Simplified NPP model adopted in this study (Kim and Lee, 2015)

Fig. 1. Beam-stick model for the seismically isolated NPP model

element of the seismic isolation (Lead Rubber Bearing, LRB) are simplified by 9 equivalent elements with the previous properties as shown in Fig. 2.

2.2 Input earthquake

The design response spectrum for the horizontal earthquake input motion at the ground surface of the free-field soil adopts the RG 1.60 design spectrum with the acceleration component at natural frequency of 25 Hz augmented by 30% and the ZPA (Zero Period Acceleration) extended from 33 Hz to 40 Hz as shown in Fig. 3(a). The acceleration time history for the seismic analysis is shown in Fig. 3(b) as provided by KEPCO E&C so as to include the design response spectrum. In addition, the displacement time history plotted in Fig. 3(c) is obtained by integrating twice the acceleration time history of Fig. 3(b). The PGAs of the input earthquakes used in the nonlinear SSI analysis and fixed-base analysis are 0.1 g, 0.2 g, 0.3 g, 0.4 g, and 0.5 g by scaling the input motion given in Fig. 3.

Table 1. Structural properties of the simplified NPP model

Node	Height from bottom of a basemat (m)	Nodal mass (ton)	Location between node	Area (m^2)	Shear area (m^2)	Moment of inertia (m^4)	Torsional moment of inertia (m^4)
(a) Containment building							
1	10.06	73.81	1 to 2	179.77	89.93, 89.93	49548.70, 49548.70	99097.40
2	13.41	147.57	2 to 3	179.77	89.93, 89.93	49548.70, 49548.70	99097.40
3	16.76	167.72	3 to 4	179.77	89.93, 89.93	49548.70, 49548.70	99097.40
4	21.03	169.38	4 to 5	179.77	89.93, 89.93	49548.70, 49548.70	99097.40
5	24.46	150.94	5 to 6	179.77	89.93, 89.93	49548.70, 49548.70	99097.40
6	27.89	287.22	6 to 7	179.77	89.93, 89.93	49548.70, 49548.70	99097.40
7	33.83	520.86	7 to 8	179.77	89.93, 89.93	49548.70, 49548.70	99097.40
8	39.93	268.33	8 to 9	179.77	89.93, 89.93	49548.70, 49548.70	99097.40
9	46.02	286.77	9 to 10	179.77	89.93, 89.93	49548.70, 49548.70	99097.40
10	52.96	305.21	10 to 11	179.77	89.93, 89.93	49548.70, 49548.70	99097.40
11	59.89	239.82	11 to 12	179.77	89.93, 89.93	49548.70, 49548.70	99097.40
12	63.86	351.94	12 to 13	45.43	72.84, 72.84	38787.13, 38787.13	77574.24
13	71.63	298.38	13 to 14	45.43	72.84, 72.84	29983.17, 29983.17	59966.33
14	79.40	299.85	14 to 15	45.43	72.84, 72.84	12273.42, 12273.42	24546.85
15	87.25	150.81					
(b) Internal structure							
101	10.06	184.53	101 to 102	833.15	662.77, 662.77	85092.78, 159793.87	164989.72
102	11.58	341.40	102 to 103	883.97	704.30, 704.30	85438.02, 163884.95	167389.13
103	13.56	796.48	103 to 104	857.92	684.03, 684.03	85248.75, 161420.20	165957.82
104	16.76	523.67	104 to 105	313.79	221.77, 221.77	16513.90, 42506.73	37753.43
105	19.05	273.11	105 to 106	254.61	176.07, 176.07	16361.05, 38885.91	35811.75
106	21.03	465.68	106 to 107	221.94	144.33, 144.33	15858.75, 38768.05	35233.94
107	24.38	296.86	107 to 108	261.38	175.93, 175.93	16413.58, 40332.65	36571.27
108	25.91	355.48	108 to 109	202.77	130.82, 130.82	16051.36, 37048.28	34566.87
109	27.89	287.22	109 to 110	202.77	130.82, 130.82	16051.36, 37048.28	34566.87
110	29.87	264.89	110 to 111	202.70	130.75, 130.75	16051.36, 37048.27	34566.86
111	33.83	520.86	111 to 112	103.23	94.90, 94.90	3221.01, 9333.40	7888.58
112	39.62	271.77	112 to 113	97.94	92.25, 92.25	3196.91, 9285.20	7840.38
113	44.50	81.39					
(c) Auxiliary building							
201	3.048	694.97	201 to 202	1598.68	727.32, 600.52	855877.71, 727529.46	270983.36
203	10.06	5663.95	204 to 205	1660.46	770.35, 611.30	939048.10, 717167.23	299661.91
206	16.76	5070.17	207 to 208	1454.40	633.41, 567.27	811754.73, 552415.01	234621.61
209	22.86	4485.33	210 to 211	1529.65	659.43, 589.38	821102.11, 603046.85	257238.81
212	28.19	3955.54	213 to 214	1363.35	565.41, 558.81	651662.24, 517191.74	234033.31
215	33.83	3023.95	216 to 217	842.17	358.88, 329.06	426491.71, 280903.29	217184.77
218	38.71	1861.69	219 to 220	579.06	212.00, 261.61	251924.95, 214924.85	95692.25
221	44.20	1805.14	222 to 223	371.98	160.35, 192.03	134196.92, 152796.02	65942.49
224	51.36	818.49					

Table 2. Natural frequency of the simplified NPP model

Structure	Original model (Hz)	Simplified model (Hz)	Remarks
Containment building	3.713	3.665	X-direction
	3.719	3.674	Y-direction
Internal structure	9.690	9.563	X-direction
	11.305	11.309	Y-direction
Auxiliary building	6.384	6.332	X-direction
	5.999	5.992	Y-direction

2.3 Soil conditions

The soil conditions adopted for the nonlinear SSI analysis using BRM are three of soil profiles taken from Han et al.[30] and names as SC1, SC2, and SC3. The properties down to the depth of 61 m (200 ft) are used for each soil in the nonlinear SSI analysis. Figs. 4 to 6 present the respective properties of the SC1, SC2, and SC3 soil profiles.

Soil profile SC1 has a shear wave velocity of 548.8 to 1862.3 m/s down to the depth of 61 m, and is the softest among the three soil profiles with a velocity of 1862.3 m/s in the semi-infinite layer. Soil

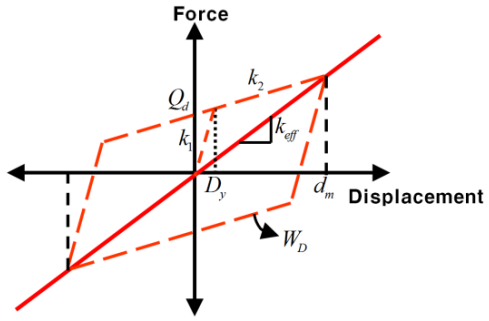

k_{eff} (kN/m)	k_1 (kN/m)	k_2 (kN/m)	Q_d (kN)	d_m (m)
3.578×10^5	2.569×10^6	1.973×10^5	3.923×10^4	0.4

(a) Properties of LRB

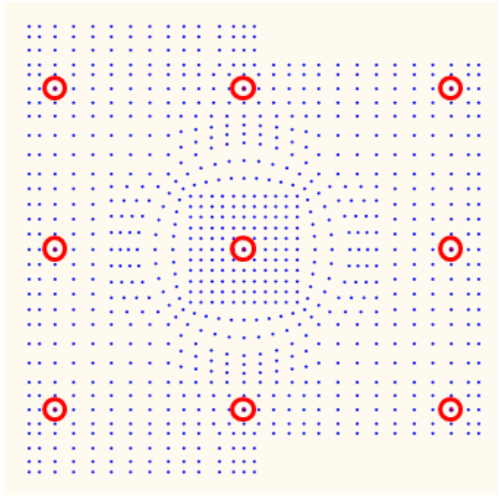

(b) Layout of LRBs

Fig. 2. Nonlinear model of seismic isolation

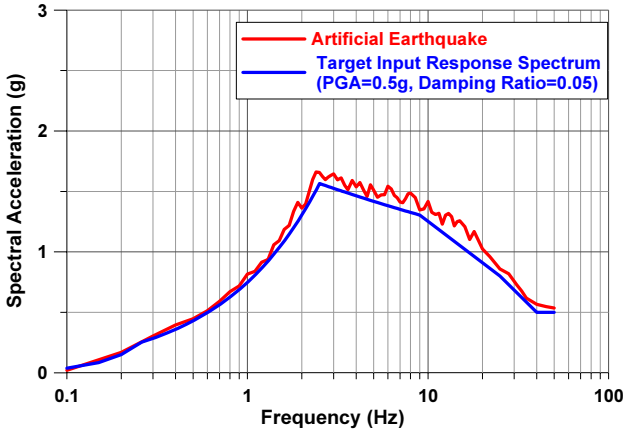

(a) Design response spectrum of input motion (PGA = 0.5 g)

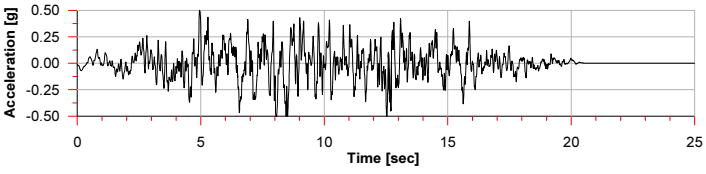

(b) Acceleration time history (PGA = 0.5 g)

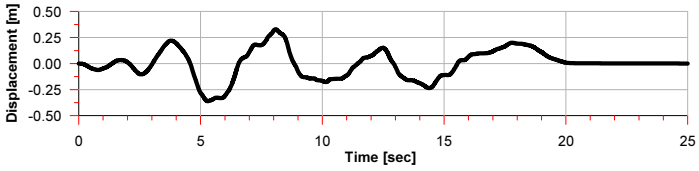

(c) Displacement time history (PGD = 0.361m)

Fig. 3. Input motion at ground surface of free-field soil

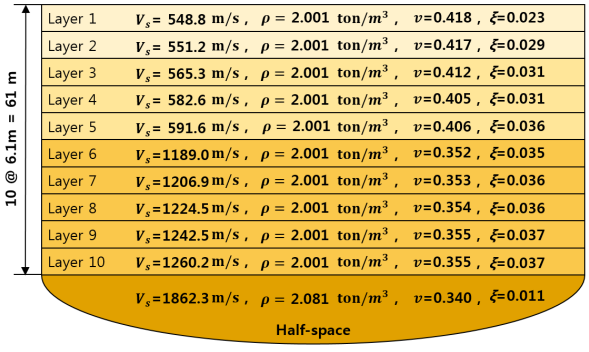

Fig. 4. Soil properties of soil profile SC1

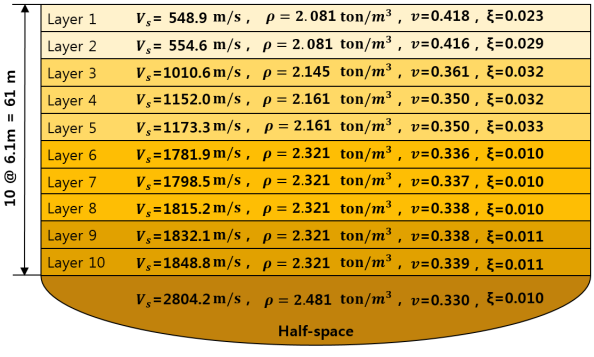

Fig. 5. Soil properties of soil profile SC2

profile SC2 has a shear wave velocity of 548.9 to 2804.2 m/s down to the depth of 61 m with a velocity of 2804.2 m/s in the semi-infinite layer. Soil profile SC3 has a shear wave velocity of 1437.1 to 2804.2 m/s down to the depth of 61 m with a velocity of 2804.2 m/s in the semi-infinite layer.

3. Nonlinear SSI analysis and fixed-base analysis

3.1 Application procedure of BRM for nonlinear SSI analysis

The concept of BRM subdivides the nonlinear SSI analysis problem

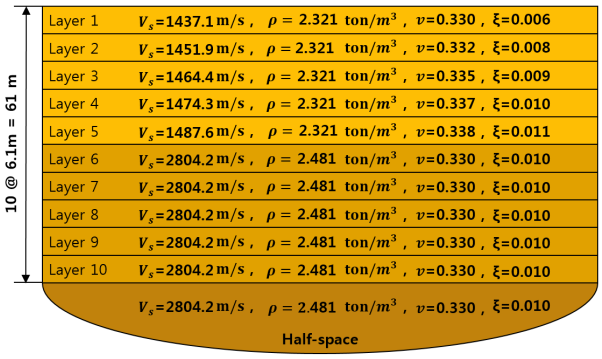

Fig. 6. Soil properties of soil profile SC3

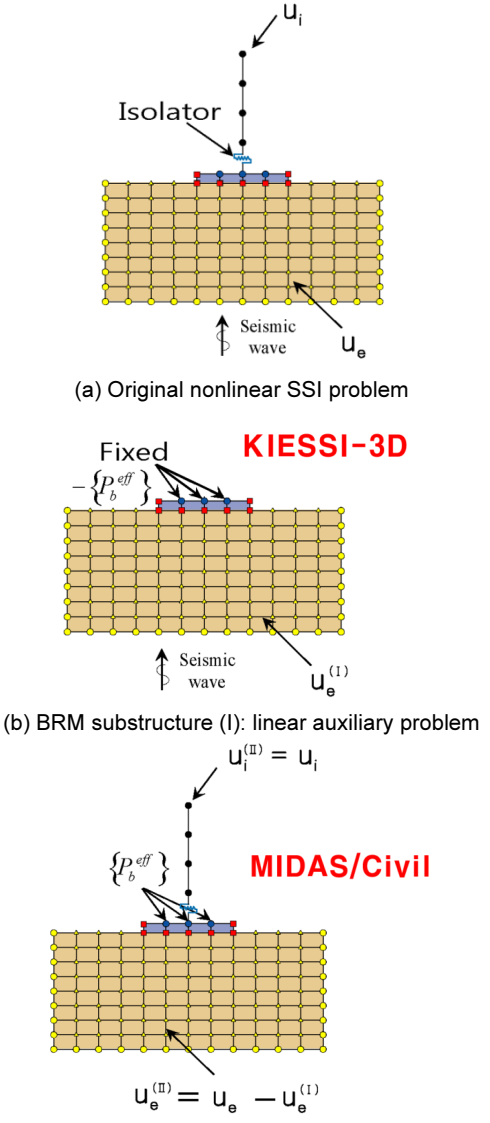

Fig. 7. Concept of BRM for nonlinear SSI analysis of base-isolated structures

of the seismically isolated nuclear structure shown in Fig. 7(a) into two substructures (I) and (II), and superposes substructure (I) shown in Fig. 7(b) in which the base of the seismic isolation is fixed and substructure (II) shown in Fig. 7(c). Here, substructure (I) constitutes the linear SSI problem while substructure (II) represents the nonlinear problem. Thus, the total solution $\mathbf{u}^t(t)$ can be obtained by simple summation as

$$\mathbf{u}^t(t) = \mathbf{u}^{(I)}(t) + \mathbf{u}^{(II)}(t) \tag{1}$$

where the superscripts (I) and (II) stand for the substructure (I) and the substructure (II) respectively; and the motions within the nonlinear body in the substructure (I) are zero, i.e.

$$\mathbf{u}_i^{(I)}(t) = \mathbf{0} \quad \text{and} \quad \mathbf{u}_b^{(I)}(t) = \mathbf{0} \tag{2}$$

Thus responses in the nonlinear region 'i' and the boundary 'b' are the same as those in the substructure (II), as follows

$$\mathbf{u}_i^t(t) = \mathbf{u}_i^{(II)}(t) \quad \text{and} \quad \mathbf{u}_b^t(t) = \mathbf{u}_b^{(II)}(t) \tag{3}$$

With this superposition, the nonlinear restoring forces in the nonlinear region 'i' and the boundary 'b' are also the same as those in the substructure (II). More detailed theoretical background are given in Reference 29.

In substructure (I) of BRM, the reactions at the interface are computed considering the dynamic characteristics of the soil by performing conventional linear SSI analysis and fixing the lower part of the seismic isolation. For this part, the linear SSI analysis program in the frequency-domain, KIESSI-3D, is applied[33,34]. Substructure (II) of BRM refers to the analysis step of the wave radiation problem which performs forced vibration analysis by applying the interfacial reactions computed at the base of the seismic isolation of substructure (I) in the opposite direction. Here, the multi-purpose finite element analysis program MIDAS/Civil[35] is used since it can take into account the nonlinearity of the seismic isolation.

In substructure (II) of BRM, need is for a program enabling to deal with the interface by means of a type of energy-absorbing boundary condition that is the PML element or damper-spring element within the analysis domain for the efficient treatment of the radial damping occurring in the SSI[27]. In this study, the boundary is modeled using damper-spring elements. The coefficients for the spring element and the viscous damper element at the boundary proposed by Deek and Randolph [36], Kellezi[37], and Liu[38] are adopted. The spring coefficient K_{BN} and damping coefficient C_{BN} in the normal direction per unit area at the boundary are computed using Eq. (4) and, the spring coefficient K_{BT} and damping coefficient C_{BT} in the tangent direction are calculated using Eq. (5).

$$K_{BN} = \frac{\rho V_p^2}{2r},\ C_{BN} = \rho V_P \quad \text{(normal direction)} \tag{4}$$

$$K_{BT} = \frac{\rho V_s^2}{2r},\ C_{BT} = \rho V_s \quad \text{(tangent directions)} \tag{5}$$

where r is the radial distance from the center of the foundation to the boundary; ρ is the mass density of the far field soil; V_p is the compression wave velocity in the far field soil; and, V_s is the shear wave velocity in the far field soil.

3.2 Establishment and verification of BRM analysis model

The nonlinearity of the seismic isolation and the soil-structure interaction should be considered for the nonlinear SSI analysis of seismically isolated nuclear facilities. The nonlinear behavior of the seismic isolation can easily be considered using a finite element program in the time domain. Therefore, the accuracy of a nonlinear SSI analysis depends on the accuracy of the boundary reaction forces calculating in frequency and a suitable numerical model for the wave radiation problem in the time domain. In order to evaluate reaction forces and the numerical model for the BRM analysis, equivalent linear time history analysis is performed and the structural responses are compared with those obtained by ordinary seismic analysis using KIESSI-3D. The analysis models for the analysis using KIESSI-3D and MIDAS/Civil are illustrated in Fig. 8. The models are prepared to meet wave passage criteria, i.e., $h \le \frac{1}{5}\frac{V_s}{f_{\max}}$, where h is the largest size of the finite element mesh; V_s is the smallest value of shear wave velocity of soil(=548.8 m/s); $f_{\max}$ is maximum frequency of interest (=12 Hz). The dashpot and spring elements are placed on the truncated FE model depicted in Fig. 8(b) in accordance to method described in the Section 3.1 to absorb the radiating elastic waves.

The seismic isolation of the equivalent linear analysis applies an effective stiffness k_{eff} and its damping is modeled by means of the viscous damping coefficient. The damping ratio $\xi_{BI} = 0.28$ is applied to compute the viscous damping coefficient c_{BI} using Eq. (6).

$$c_{BI} = 2\xi_{BI}\sqrt{m\,k_{eff}} \tag{6}$$

where ξ_{BI} is the critical damping ratio of the base isolator; k_{eff} is the effective stiffness of the seismic base isolation (Fig. 2); and, m = 5.171×10^4 ton is the mass of the superstructure for one base isolation.

The reactions at the boundary applied as effective loads in substructure (II) of BRM are calculated using KIESSI-3D for the soil profiles SC1, SC2 and SC3 at the 9 spots at the base of the base isolators (BI) shown in Fig. 9. Fig. 10 plots the reactions at BI of Fig. 9.

The time-domain analysis using MIDAS/Civil operates by the direct integration method. Here, the damping ratio of the structure and soil at the exception of the base isolation is the Rayleigh damping, that is $[C] = \alpha[M]+\beta[K]$. For the calculation of the Rayleigh damping of the structures, a damping proportional to the stiffness by a constant of proportionality β is applied giving a damping ratio of 0.05 at 3.67 Hz for the containment building, 0.07 at 6.33 Hz for the auxiliary building, and 0.07 at 9.56 Hz for the internal structure. Frequencies of 0.4 Hz and 10.0 Hz are applied for the calculation of the Rayleigh damping of the

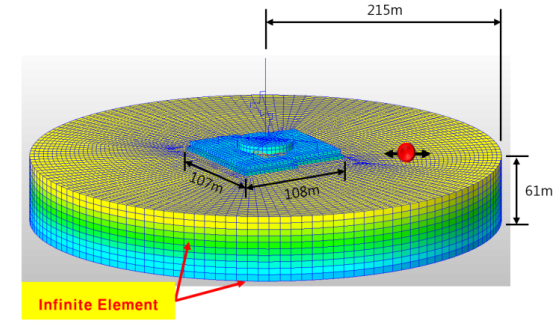

(a) KIESSI-3D model

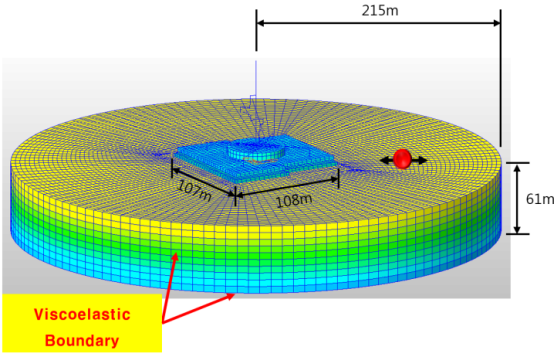

(b) MIDAS/Civil model

Fig. 8. Numerical models for seismically isolated NPP structure

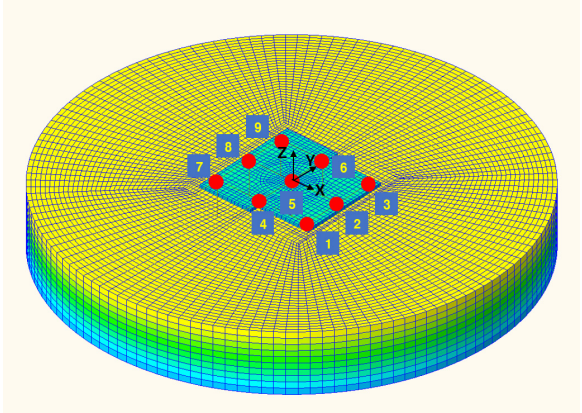

Fig. 9. KIESSI-3D model for calculating reaction forces at fixed supports of base isolator due to vertically incident SV-waves in x-z plane

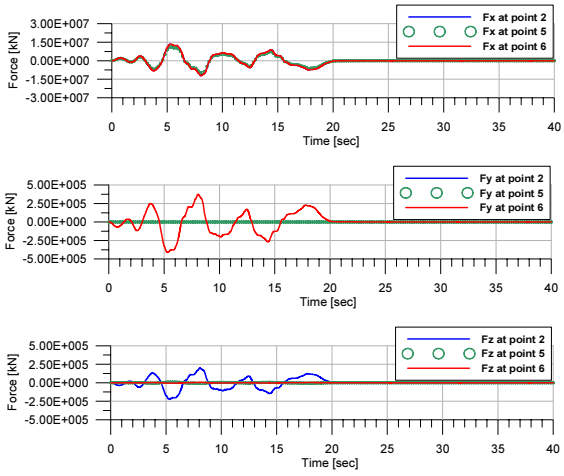

(a) Soil profile SC1

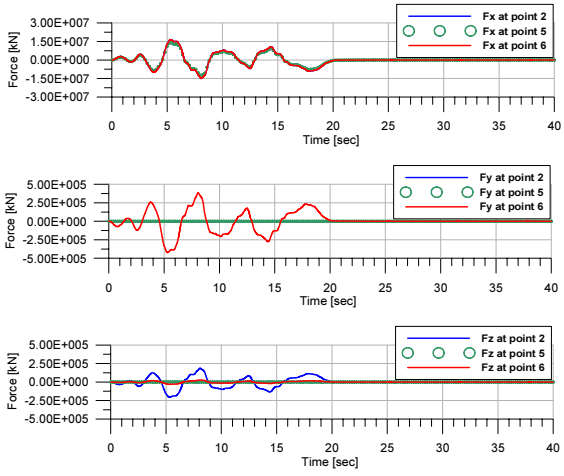

(b) Soil profile SC2

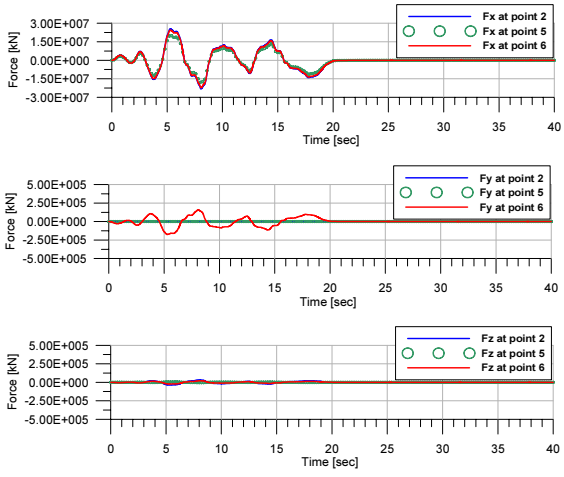

(c) Soil profile SC3

Fig. 10. Reaction forces at selected points (2, 5 and 6 in Fig. 9) of fixed support of base-isolator due to vertically incident SV-waves in x-z plane

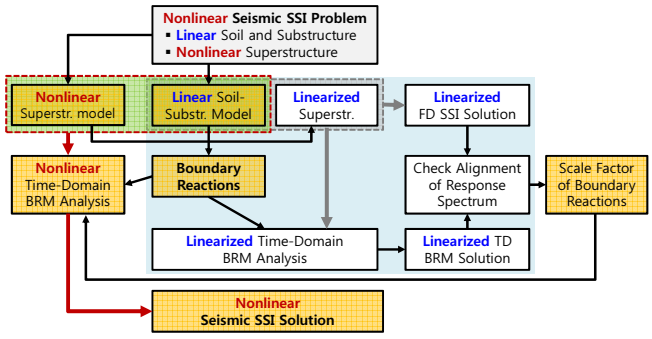

Fig. 11. Flow diagram of nonlinear SSI analysis by BRM

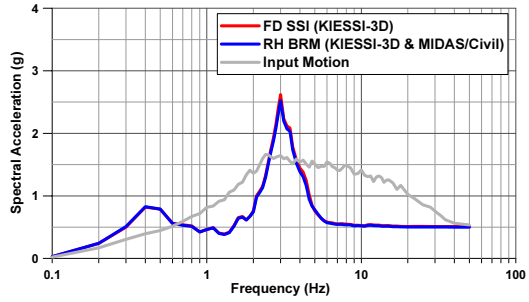

(a) Horizontal responses at the top of containment for soil profile SC1 (5% damping ratio, PGA = 0.5 g)

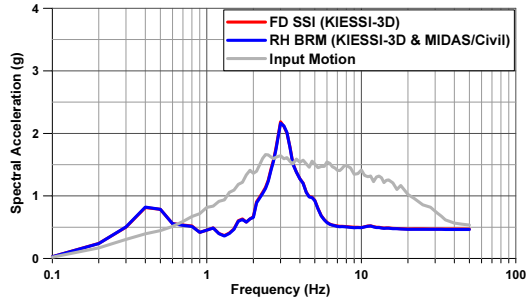

(b) Horizontal responses at the top of containment for soil profile SC2 (5% damping ratio, PGA = 0.5 g)

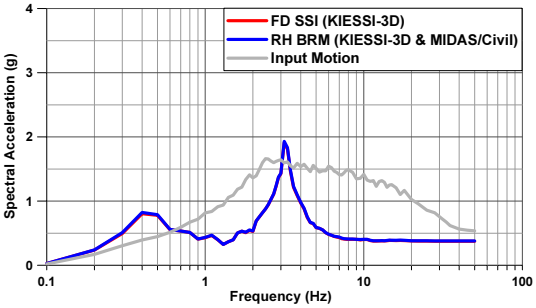

(c) Horizontal responses at the top of containment for soil profile SC3 (5% damping ratio, PGA = 0.5 g)

Fig. 12. Comparison of response spectra for horizontal response of the equivalent linear NPP model (frequency-domain SSI analysis vs. response history BRM analysis)

soil, and particular damping ratio is adopted for each soil profile. The structural response of the equivalent linear analysis in the frequency-domain using KIESSI-3D is used as solution of reference. Identically to BRM analysis, the analysis using KIESSI-3D applies the Rayleigh damping for the structures and soil, and adopts viscous damping for the seismic base isolation.

In this study, calibration of the boundary reactions was conducted for the equivalent linear problem prior to the time-domain nonlinear analysis by BRM (Fig. 11). The scale factor for the boundary reactions

was determined with reference to the response spectrum of the superstructure obtained by the frequency-domain SSI analysis at the frequency of the base isolation (0.40 Hz in this example).

Fig. 12 compares the horizontal response spectra at the top of the containment building obtained by equivalent linear analysis by BRM and by equivalent linear SSI analysis in frequency-domain. The reliability of the BRM numerical model for the nonlinear analysis can be verified through the good agreement between the linear analysis results by BRM and the linear SSI analysis results in the frequency domain for each of the considered soil profiles.

3.3 Comparison of responses by nonlinear SSI analysis and fixed-base analysis

Nonlinear SSI analysis using BRM and nonlinear time history analysis assuming a fixed-base without consideration of the soil profile were carried out for the seismically isolated structure. The BRM analysis model for the nonlinear SSI analysis is identical to the linear analysis model except for the nonlinear elements of the base isolation. The fixed-base analysis model corresponds to the simplified model of the seismically isolated NPP model in Fig. 1(b) in which the base is fixed.

In a seismically isolated structure, the seismic load acting on the structure generally reduces but the displacement of the superstructure augments. This implies that the displacement of the base isolation constitutes an important design variable. In this study, the response at the top of the structure and the peak displacement of the base isolation are computed with respect to the PGA of the input control motion by means of the nonlinear SSI analysis using BRM and the fixed-base analysis.

Fig. 13 compares the horizontal acceleration response spectra with the results of the fixed-base analysis according to the soil conditions of BRM. Figs. 14 to 16 plot the nonlinear hysteresis curves of the base isolation. Table 3 arranges the peak displacements of the base isolator obtained by means of the two types of analysis.

In Fig. 13, it can be seen that, for soil profile S9 with the closest soil condition to the fixed-base, the responses at the top of the structure given by both types of analysis are very similar when the intensity of the seismic load is relatively small (PGA = 0.1 g and 0.3 g). However, the comparison of the spectral acceleration response given by the fixed-base analysis to that given by the nonlinear SSI analysis in case of strong seismic load (PGA = 0.5 g) with damping ratio of 5% in Fig. 13(c) reveals that there is very minimal difference at natural frequency of about 0.4 Hz for the seismic isolation whereas the response becomes smaller by approximately 10.0% at natural frequency of about 3.0 Hz for the superstructure.

Besides, for the soil profiles SC1 and SC2, it appears in Fig. 13(a) and 13(b) that the fixed-base response is very close to the SSI response at the natural frequency of the base isolation whereas the spectral acceleration response exhibits clear difference at the natural frequency of the superstructure and at frequency range higher than 2 Hz and that this difference accentuates with larger intensity of the seismic input. On the whole, it can be observed that the fixed-base response is smaller than the SSI response.

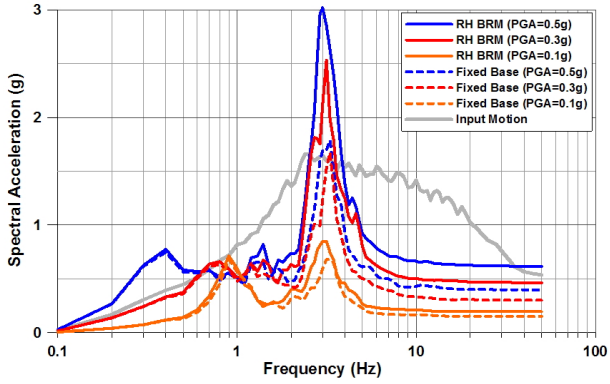

(a) Horizontal responses at the top of containment for soil profile SC1 (5% damping ratio)

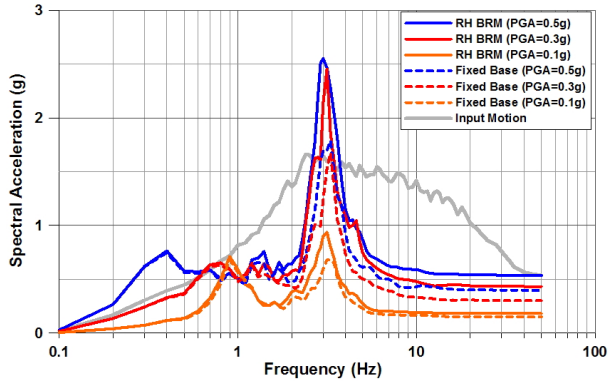

(b) Horizontal responses at the top of containment for soil profile SC2 (5% damping ratio)

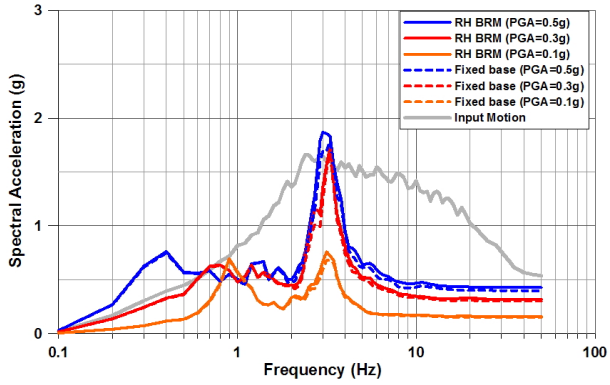

(c) Horizontal responses at the top of containment for soil profile SC3 (5% damping ratio)

Fig. 13. Response spectra for horizontal response of seismically isolated NPP structure (frequency-domain SSI analysis vs. response history BRM analysis)

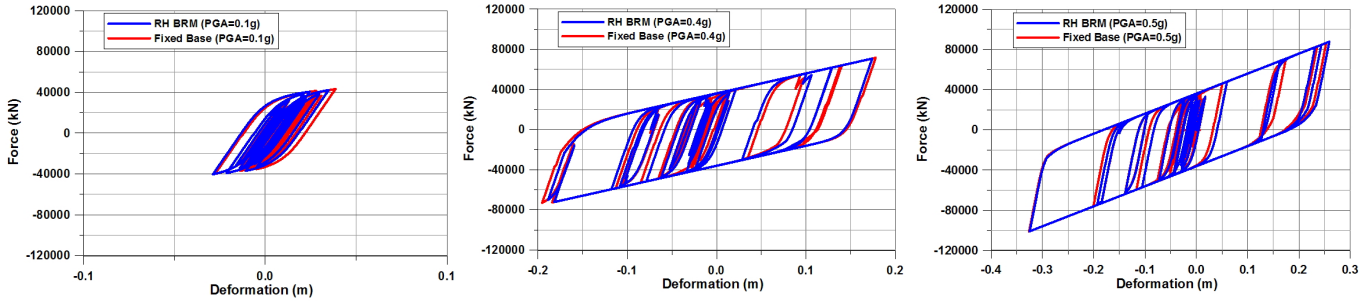

(a) Input motion with PGA = 0.1 g (b) Input motion with PGA = 0.4 g (c) Input motion with PGA = 0.5 g

Fig. 14. Nonlinear hysteresis curves of seismic isolator for soil profile SC1

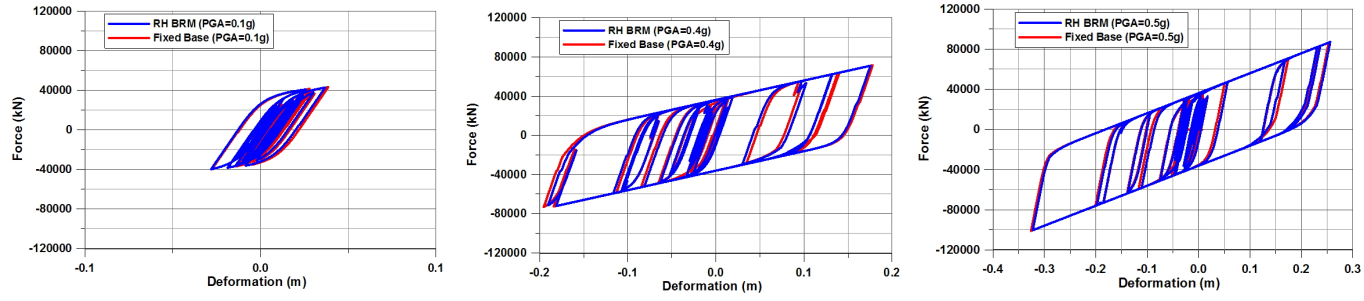

(a) Input motion with PGA = 0.1 g (b) Input motion with PGA = 0.4 g (c) Input motion with PGA = 0.5 g

Fig. 15. Nonlinear hysteresis curves of seismic isolator for soil profile SC2

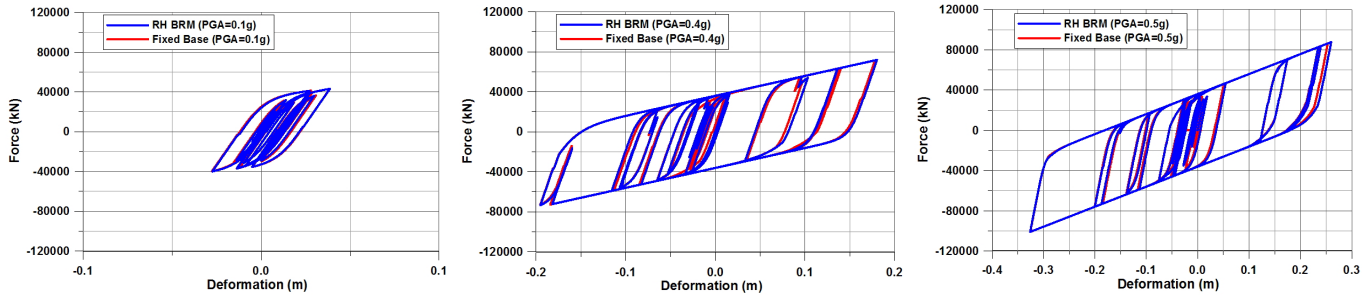

(a) Input motion with PGA = 0.1 g (b) Input motion with PGA = 0.3 g (c) Input motion with PGA = 0.5 g

Fig. 16. Nonlinear hysteresis curves of seismic isolator for soil profile SC3

Table 3. Peak displacement of seismic isolator (in mm)

Analysis case	PGA of input motion				
	0.1 g	0.2 g	0.3 g	0.4 g	0.5 g
Fixed-base	39 (1.000)	86 (1.000)	142 (1.000)	195 (1.000)	326 (1.000)
Nonlinear SSI (soil profile SC1)	35 (0.903)	85 (0.985)	135 (0.954)	174 (0.892)	325 (0.996)
Nonlinear SSI (soil profile SC2)	37 (0.955)	84 (0.975)	136 (0.963)	181 (0.928)	323 (0.990)
Nonlinear SSI (soil profile SC3)	39 (1.000)	86 (1.000)	141 (0.993)	195 (1.000)	326 (1.000)

Note: values in parenthesis = ratios to fixed-base result.

Fig. 17 compares the peak displacement of the base isolator according to the eventual consideration of SSI and the intensity of the seismic input load. It can be observed that the peak displacement of the base isolator provided by the fixed-base analysis is similar or slightly larger than that given by the nonlinear SSI analysis.

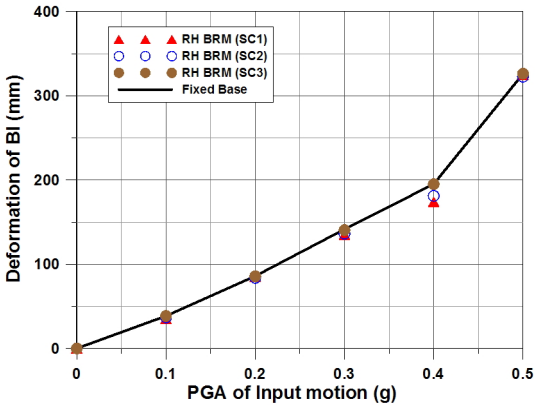

Fig. 17. Peak deformation of seismic isolator according to PGA of input control motion

4. Conclusions

In a will to evaluate the conservativeness of the fixed-base analysis as compared to the soil-structure interaction (SSI) analysis for a base-isolated model, this study conducted nonlinear SSI analysis using BRM (Boundary Reaction Method) and fixed-base analysis on a seismically isolated model of a nuclear power plant. The reliability of BRM was secured through the verification of the numerical model with an equivalent linear base isolation model. Nonlinear SSI analysis was performed considering 3 types of soil profile and 5 different intensities of the seismic load. The response at the top of the structure and the peak deformation of the base isolation obtained by the nonlinear SSI analysis and the fixed-base analysis were compared for each considered analysis condition. The following conclusions can be drawn from the analysis results.

1) In view of the nonlinear displacement of the base isolation, the response provided by the fixed-base condition appeared to be larger and the difference tended to accentuate with higher intensity of the input ground motion. It can thus be stated that the analysis results for the seismically isolated structure assuming fixed base lead to conservative computation of the design displacement of the base isolation in the seismically isolated nuclear facilities.
2) With regard to the floor response spectrum of the superstructure, both fixed-base condition and SSI condition were seen to provide similar results in case of hard soil and small input motion but the difference in the response increased with higher intensity of the input ground motion and softer soil. Moreover, the floor response spectrum under fixed-base condition was smaller than that under SSI condition.

Finally, further studies incorporating actual ground accelerations are recommended to enhance the above conclusions.

/ ACKNOWLEDGEMENTS /

This work was supported by the Nuclear Power Core Technology Development Program of the Korea Institute of Energy Technology Evaluation and Planning (KETEP), granted financial resource from the Ministry of Trade, Industry & Energy, Republic of Korea. (No.2014151010170B)

/ REFERENCES /

1. Mayes RL, Buckle IG, Kelley TE, Jones LR. AASHTO seismic isolation design requirements for highway bridges. J. Struct. Eng.-ASCE. 1992;118:284-304.
2. Walters M, Honeck B, Elsesser E. Use of seismic isolation in new and retrofit construction, Proc. Joint ASME/JSME Pressure Vessels and Piping Conference, Seismic, Shock and Vibration Isolation, Honolulu, HI. 1995;PVP319:31-38.
3. Ebisawa K, Ando K, Shibata K. Progress of a research program on seismic base isolation of nuclear components. Nucl. Eng. Des. 2000;198:61-74.
4. Yoo B, Lee JH, Koo GH, Lee HY, Kim JB. Seismic base isolation technologies for Korea advanced liquid metal reactor. Nucl. Eng. Des. 2000;262:429-434.
5. Wang H, Weng D, Lu X, Lu L. Life-cycle cost assessment of seismically base-isolated structures in nuclear power plants. Nucl. Eng. Des. 2013;262:429-434.
6. Chen J, Zhao C, Xu Q, Yuan C. Seismic analysis and evaluation of the base isolation system in AP1000 NI under SSE loading. Nucl. Eng. Des. 2014;278:117-133.
7. Forni M, Poggianti A, Dusi A. Seismic isolation of nuclear power plant. Proc. 15th WCEE, Lisbon, 2012 September 24-28. c2012.
8. ASCE 4-12. Seismic analysis of safety-related nuclear structures and commentary. Draft Revision 16; ASCE; c2012.
9. Coleman J, Jeremic B, Whittaker A. Nonlinear time domain seismic soil structure interaction (SSI) analysis for nuclear facilities and draft appendix B of ASCE 4. SMiRT-22, San Francisco, CA, 2013 August 18-23. c2013.
10. NUREG-xxxx, Technical consideration for seismic isolation of nuclear facilities, draft. U.S. NRC. c2013.
11. Stehmeyer (III) EH, Rizos DC. Considering dynamic soil structure interaction (SSI) effects on seismic isolation retrofit efficiency and the importance of natural frequency ratio. Soil. Dyn. Earthq. Eng. 2008;28:468-479.
12. Spyrakos CC, Koutromanos IA, Maniatakis CA. Seismic response of base-isolated buildings including soil-structure interaction. Soil. Dyn. Earthq. Eng. 2009;29(4):658-668.
13. Alavi E, Alidoost M. Soil-structure interaction effects on seismic behavior of base-isolated buildings. Proc. 15th WCEE, Paper No. 4982; 2012 September 24-28; Lisbon, Portugal. c2012.

14. Jarernprasert SE, Bazan-Zurita E, Bielak J. Seismic soil-structure interaction response of inelastic structures. Soil. Dyn. Earthq. Eng. 2013;47:132-143
15. Karabork T, Deneme IO, Bilgehan RP. A comparison of the effect of SSI on base isolation systems and fixed-base structures for soft soil. Geomechanics and Engineering. 2014;7(1):87-103.
16. Rochal LEP, Colunga AT, Cordero C. Influence of site effects and soil-structure interaction on seismic isolation of buildings on soft soils. Proc. Tenth U.S. National Conference on Earthquake Engineering, Frontiers of Earthquake Engineering, 2014 July 21-25, Anchorage, Alaska. c2014.
17. Luco JE. Effects of soil-structure interaction on seismic base isolation. Soil. Dyn. Earthq. Eng. 2014;66:167-177.
18. Kawamoto JD. Solution of nonlinear dynamic structural system based on a hybrid frequency-time-domain approach. Research Report R83-5, MIT, Dept. of Civil Eng., Cambridge, MA. c1983.
19. Bernal D, Youssef A. A hybrid time frequency domain formulation for non-linear soil-structure interaction. Earthq. Eng. Struct. Dyn. 1998;27:673-685.
20. Kim JM, Choi JS, Lee JS. A new hybrid method for nonlinear soil-structure interaction analysis. J. Earthq. Eng. Soc. Korea. 2003;7:1-7.
21. Bielak J, Loukakis K, Hisada Y, Yoshimura C. Domain reduction method for three-dimensional earthquake modeling in localized regions. Part I: theory. Bull. Seismol. Soc. Am. 2003;93:817-824.
22. Basu U. Explicit finite element perfectly matched layer for transient three-dimensional elastic waves. Int. J. Numer. Meth. Eng. 2009;77:151-176.
23. Solberg JM, Hossain Q, Blink JA, Bohlen SR, Mseis G, Greenberg H. Development of a generalized methodology for soil-structure interaction analysis using nonlinear time-domain techniques. Report # LLNL-TR-635762, Lawrence Livermore National Laboratory. c2013.
24. Tafazzoli N, Pisano F, Abbel JA, Kamrani B, Jeong CG, Aldridge B, Roche R, Kammerer A, Jeremic B. The NRC ESSI simulator program current status. SMiRT-22, 2013 August 18-23, San Francisco, CA.
25. LSTC, LS-DYNA user's manual, Vols. 1 & 2, Version 971 R5. c2010.
26. Kim JM, Lee EH. Boundary reaction method for nonlinear soil-structure interaction analysis. Proc. KSCE Confer. c2013.
27. Lee GH, Hong KY, Lee EH, Kim JM. Verification of linear FE model for nonlinear SSI analysis by boundary reaction method. . Computational Structural Engineering Institute of Korea. 2014a; 27:95-102.
28. Lee EH, Kim JM, Lee SH. Nonlinear soil-structure interaction analysis of a seismically isolated nuclear power plant structure using the boundary reaction method. J. Earthq. Eng. Soc. Korea. 2015;19:37-43.
29. Kim JM, Lee EH, Lee SH. Boundary reaction method for nonlinear soil-structure interaction under earthquake loads. Soil Dyn. Earthq. Eng. 2016; Under review.
30. Han SR, Nam MJ, Seo CG, Lee SH. Soil-structure interaction analysis for base-isolated nuclear power plants using an iterative approach. J. Earthq. Eng. Soc. Korea. 2015;19:21-28.
31. Lee MH, Song JK, Lee EH. Multi-step analysis of seismically isolated NPP containment structures with lead-rubber bearings. J. Earthq. Eng. Soc. Korea. 2014b;18:261-269.
32. Kim JM, Lee EH. Development and verification of simplified beam-stick model of seismically isolated APR1400 nuclear power plant structure. Research Report, Central Research Institute of KHNP. 2015; KETEP Project No. 2014151010170B. c2015.
33. Yun CB, Chang SH, Seo CG, Kim JM. Dynamic infinite elements for soil-structure interaction analysis in a layered soil medium. Int. J. Struct. Stab. Dy. 2007;7(4):693-713.
34. Ryu JS, Seo CG, Kim JM, Yun CB. Seismic response analysis of soil-structure interactive system using a coupled three-dimensional FE-IE method. Nucl. Eng. Des. 2010;240:1949-1966.
35. MIDAS/Civil, Available from: http://www.midasit.com/
36. Deek AJ, Randolph MF. Axisymmetric time domain transmitting boundaries. J. Eng. Mech.-ASCE. 1994;120:25-42.
37. Kellezi L. Local transmitting boundaries for transient elastic analysis. Soil. Dyn. Earthq. Eng. 2000;19:533-547.
38. Liu J, Gu Y, Wang Y, Li B. Efficient procedure for seismic analysis of soil-structure interaction system. Tsinghua Science and Technology. 2006;11:625-631.